

Peer review status:

This is a non-peer-reviewed preprint submitted to EarthArXiv.

# Aquascan: Graph-Based Learning for Distributed Marine Sensing

Abel Dantas  
ProDEI, Universidade do Porto & CTVC  
adantas@ctvc.pt

May 2025

## Abstract

Marine monitoring faces unprecedented challenges as climate change and human activities reshape ocean ecosystems. Traditional tracking methods struggle with the scale and complexity of modern marine sensing needs. This paper proposes distributed networks of low-cost drifting sensors and presents a comparative study of heterogeneous graph neural networks (GNNs) versus Kalman filters for predicting marine entity trajectories in such distributed networks with intermittent observations. Using the Aquascan simulation framework, we model drifting sensors detecting marine entities across 480 km<sup>2</sup> of ocean surface with realistic movement patterns and sparse coverage. Experiments across multiple prediction horizons show GNNs significantly outperform Kalman filters: GNNs maintain >95% AUC (Area Under the Curve) across all horizons while Kalman filters degrade from 97% to 69% AUC. The performance gap widens under challenging conditions—at 5km sensor spacing, GNNs achieve 92.8% AUC versus 66.9% for Kalman filters. GNNs’ superior performance stems from leveraging network topology and reasoning about non-detections to infer entity presence in coverage gaps. These results demonstrate that graph-based approaches offer substantial advantages for distributed marine monitoring.

**Keywords:** Graph Neural Networks, Trajectory Prediction, Marine Monitoring, Heterogeneous Graphs

## 1 Introduction

Marine environments face increasing pressures from human activities, with 38.1% of the global population (2.86 billion people) living within 100 km of coastlines [1]. Marine economic activities are projected to double to \$3 trillion by 2030 [2], potentially impacting ecosystem stability through industrial expansion in offshore zones. A significant contributor to this transformation is the growth in offshore renewable energy, particularly wind power. Offshore wind capacity is projected to increase 15-fold by 2040 [3]. In Europe, implementation plans target **111 GW by 2030** [4], representing substantial changes to marine spatial use patterns.

These industrial developments intersect with shipping routes, commercial fishing, and coastal tourism, creating competing demands for maritime space [5]. Traditional coastal communities must adapt as fishing areas overlap with renewable energy installations [6]. Current monitoring infrastructure [7, 8] provides limited coverage for tracking cumulative ecosystem impacts and marine spatial planning. This observation gap manifests across multiple domains: wildlife migration patterns remain poorly understood, vessel movements in protected areas go undetected, and critical infrastructure like offshore wind turbines and oil platforms lack continuous monitoring for preventive maintenance. Additionally, an estimated **20% of global fish catches are unreported** [9, 10]<sup>1</sup>, exemplifying the broader challenge of inadequate marine sensing capa-

---

<sup>1</sup>The exact extent of unreported fishing remains uncertain. A comprehensive 2016 study suggested that unreported catches could be as high as 30% when including artisanal, subsistence, and discarded catches [11].

bilities.

Traditional approaches to marine trajectory prediction rely heavily on Kalman filters and their variants (e.g., EKF, UKF), used in marine navigation to track vessels, underwater vehicles, and buoys. While Kalman filters perform well with cooperative targets like ships broadcasting AIS data [12–14], they struggle with non-instrumented targets—particularly marine wildlife, which constitutes the primary focus of ecological monitoring efforts. Even dual Kalman configurations fail beyond short-term predictions [15], unable to capture schooling behavior, predator-prey interactions, or responses to environmental stimuli. This limitation stems from Kalman filters’ fundamental design for tracking individual entities with predefined motion models, whereas marine animal movements emerge from complex multi-agent interactions that violate the filters’ independence assumptions.

This raises our central **research question**: *Can heterogeneous Graph Neural Networks (GNNs) outperform traditional Kalman filters for trajectory prediction in distributed marine sensing networks with intermittent observations?* Specifically, we investigate:

1. How do GNNs and Kalman filters compare in accuracy across different prediction horizons?
2. To what extent can GNNs leverage network topology and multi-hop information propagation to maintain prediction accuracy when direct observations are sparse?

This study addresses these questions by evaluating whether heterogeneous Graph Neural Networks (GNNs) can predict multi-entity marine motion more accurately than Kalman filters in non-cooperative sensing scenarios characterized by partial observability and sensor drift. Using the Aquascan simulation framework, we modeled multi-entity behavior with distributed sensing and trained a GraphSAGE model for link prediction on spatiotemporal graphs. The research applies GNNs to non-instrumented targets—primarily marine wildlife but applicable to any untagged marine entity—by leveraging relational patterns across sensors to infer future positions,

even when direct observations are sparse or delayed.

Our work makes three key contributions:

- **Empirical comparison:** We present the first head-to-head evaluation of **Graph Neural Networks** and Kalman filters for non-cooperative marine tracking.
- **Simulation framework:** We introduce the **Aquascan** framework for modeling complex, multi-entity marine behavior with distributed sensing, enabling reproducible benchmarking of learning-based prediction methods.
- **Passive multi-target tracking:** We explore the feasibility of tracking **non-instrumented targets** via passive sensing—from marine wildlife and unauthorized vessels to drifting objects near offshore infrastructure—contrasting this with traditional approaches that rely on active transponders or tagging.

The remainder of this paper is organized as follows: Section 2 presents the Aquascan system architecture and simulation framework. Section 3 details our methodology, including the GNN architecture and baseline implementations. Section 4 describes the experimental setup and evaluation protocols. Section 5 presents results comparing GNN and Kalman filter performance. Section 6 positions our work within the broader literature. Section 7 discusses implications and limitations. Section 8 concludes with future research directions.

## 2 System Architecture and Implementation

### 2.1 Architecture

The Aquascan framework implements a hierarchical marine sensing network composed of three distinct node types. At the edge of this network,  $\epsilon$ -**nodes** function as mobile sensors deployed as drifting or anchored buoys, capable of detecting marine entities in their proximity using multi-modal sensing technologies (e.g., hydrophones and low-power sonar). These lightweight, low-power devices form the

sensory field of the network, continuously capturing local environmental signals and marine activity through passive observation.

Acting as the communication backbone,  $\sigma$ -nodes are larger fixed buoys positioned to serve as data aggregation hubs. These nodes relay information from clusters of  $\varepsilon$ -nodes, bridging the gap between edge sensors and centralized data-processing infrastructure. Finally,  $\Omega$ -nodes represent datacenters—typically onshore, but potentially offshore [16]—that aggregate the collected data and execute our predictive models, transforming raw detection events into actionable intelligence about marine ecosystem dynamics.

Power efficiency serves as the primary driver for this hierarchical architecture. Marine deployments face unique energy constraints: solar panels must withstand storms, batteries degrade in saltwater environments, and maintenance visits are costly and weather-dependent. These constraints shaped every architectural decision. The lightweight  $\varepsilon$ -nodes minimize power consumption through passive sensing and short-range communication, while  $\sigma$ -nodes concentrate power-hungry long-range transmission capabilities. This separation allows us to deploy many more low-cost  $\varepsilon$ -nodes with minimal power requirements, achieving wider coverage and finer spatial resolution than would be possible with fewer, more expensive fully-equipped buoys, while investing in robust power systems only for the critical  $\sigma$ -node infrastructure. The sparse communication topology (detailed in Section 2.6) further reduces transmission power by limiting each node to essential connections.

Figure 1 shows the heterogeneous graph structure used in our framework. This structure enables rich relational modeling: the current implementation uses communication and historical detection edges as input features, while the model learns to predict future *will\_detect* edges.

## 2.2 Core Protocols

To structure and simulate distributed marine sensing at scale, the Aquascan architecture defines three core protocol abstractions. These protocols are designed to be hardware and situation-agnostic while capturing essen-

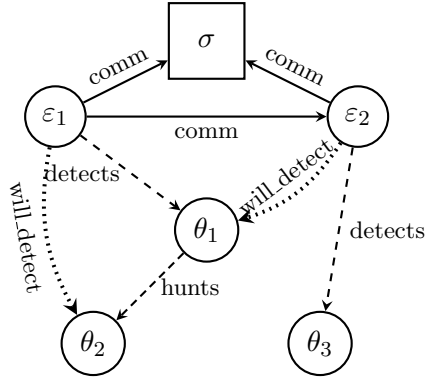


Figure 1: Simplified heterogeneous graph structure used in Aquascan, illustrating node types ( $\sigma$ : hubs,  $\varepsilon$ : sensors,  $\theta$ : entities) and edge types. The *will\_detect* edges represent future detection predictions that the model learns to predict but are not included as input during training. The *hunts* edge represents a potential future extension for modeling predator-prey relationships.

tial properties required for effective modeling. Each protocol addresses a distinct functional layer: sensing, communication, and persistence.

The **Spatiotemporal Contact Volume (SCV)** serves as our unified data abstraction, transforming multi-modal sensor detections into standardized records. Each SCV encapsulates key information about a detection event, including the detecting sensor’s identifier, timestamp, detected entity classification, position coordinates, estimated biomass volume, and species identification<sup>2</sup> when available. This abstraction allows heterogeneous sensor types to contribute to a coherent data stream, as illustrated by the following example:

```
{
  "epsilon_id": "e-0231",
  "timestamp": 123456789,
  "theta_id": "089",
  "position": {"x": 14432.7, "y": 8312.4},
```

<sup>2</sup>This paper does not prescribe specific sensor combinations or outline individual sensor functionality—hence the SCV abstraction. However, to contextualize these capabilities, one could imagine species identification at the edge involving multiple complementary sensors: sonar for acoustic signatures, optical cameras for visual features, and hydrophones for vocalizations, each potentially running lightweight ML models (e.g., YOLOv5n for real-time object detection on image streams) to extract relevant features before data fusion.

```

"estimated_volume": 17.3,
"confidence": 0.9,
"entity_type": "Dicentrarchus labrax"
}

```

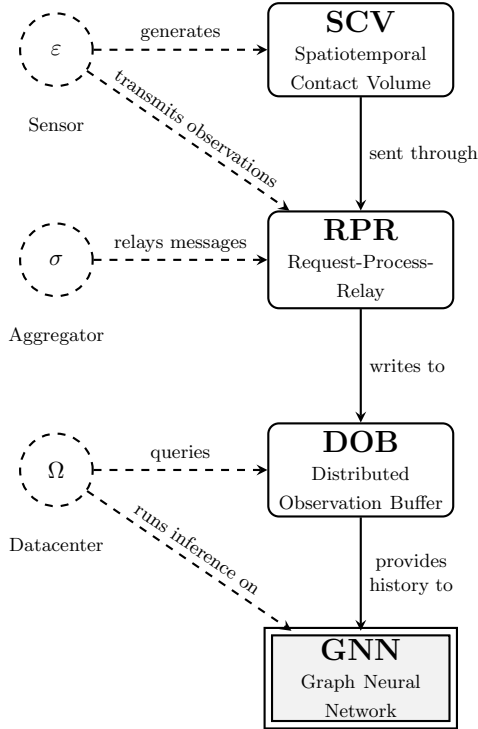


Figure 2: Core protocol abstractions showing the data flow from sensing to prediction. The SCV provides a unified data format, RPR enables efficient communication across the network, and DOB manages distributed storage with temporal indexing. Example: A sonar-equipped  $\varepsilon$ -node detects a fish school, creates an SCV with position and count data, the RPR protocol transmits it through  $\sigma$ -nodes to neighboring sensors, and the DOB stores the observation for subsequent GNN-based trajectory prediction.

Complementing SCV, the **Reliable Proximity Relay (RPR)** models communication within the distributed sensor network. RPR formalizes hop-based message passing subject to spatial and temporal constraints. Each  $\varepsilon$ -node maintains communication links to peers within a defined transmission radius  $r_{\max}$ , and may extend communication up to an emergency range  $r_{\text{emerg}}$  under exceptional conditions. For instance, during severe weather events, ocean currents can displace buoy-mounted sensors beyond their normal operational spacing. When a node detects it is losing contact with its neighbors (link quality degrading below threshold  $\tau_{\text{link}}$ ), it automatically increases transmission power to reach  $r_{\text{emerg}}$ , ensuring critical observations—such as extreme wave heights or rapid temperature changes—are not lost during the storm when data is most valuable. Additionally, RPR incorporates a positional uncertainty parameter  $\delta_{\text{pos}}$ , representing the maximum positional error bound for node localization relative to true coordinates. These parameters are left abstract at the protocol level to support a range of deployment contexts and hardware capabilities; in this study, we instantiate  $r_{\max} = 5$  km,  $r_{\text{emerg}} = 10$  km, and  $\delta_{\text{pos}} = 0$  (perfect positioning) to reflect realistic bounds for low-power long-range protocols such as LoRa<sup>3</sup> while simplifying the spatial analysis. To accommodate intermittent connectivity, RPR guarantees partial synchrony.

Finally, the **Distributed Observation Buffer (DOB)** provides persistent, time-ordered logging at each node. DOBs serve both as temporary caches and as local sources of historical context for inference. While our implementation uses a simple FIFO (First-In, First-Out) order<sup>4</sup> buffer with size constraints, the DOB is compatible with more advanced mechanisms—such as the use of Conflict-Free Replicated Data Types (CRDTs) [17]—to en-

<sup>3</sup>low-power, wide-area (LPWA) networking protocol designed to wirelessly connect battery operated devices

<sup>4</sup>Items are processed or dispatched in the same order they were received.

able progressive, mergeable aggregation of observations across the network. However, for now, the goal with DOB is not to prescribe a particular strategy, but to provide a minimal abstraction that supports system-level persistence.

### 2.3 Implementation

To compare GNN and Kalman filter performance, we implemented a representative subset of the full architecture that captures the essential dynamics while maintaining computational feasibility. Our simulation encompasses  $\epsilon$ -nodes arranged in a hexagonal grid pattern covering approximately  $30\text{ km} \times 16\text{ km}$  of ocean surface. Within this region, we simulate **15–20**  $\theta$ -nodes representing various marine entities<sup>5</sup>, each following species-specific motion models incorporating non-linear movement patterns.

Entity detection occurs when a marine entity enters a sensor’s configured sensing radius—set to 200 m at SCV instantiation time. This leads to sparse, intermittent observations with significant coverage gaps, as shown in Figure 3. Communication links are not determined by distance thresholds alone but follow a structured network topology, detailed in the next section.

To focus our investigation on the core research question—comparing predictive model performance on heterogeneous spatiotemporal graphs—we introduce several simplifications. The  $\sigma$  and  $\Omega$  layers are abstracted away, assuming direct access to sensor data for analysis. The RPR protocol is reduced to binary connectivity decisions based solely on pairwise distance, omitting multi-hop routing and communication delays. We require reliable data persistence and transmission<sup>6</sup>, abstract-

<sup>5</sup>This range was chosen primarily for visual debugging clarity. While real marine environments would contain significantly more entities (50-100+ in similar areas), the 30:1 sensor-to-target ratio allows clear visualization of individual trajectories and detection events in our simulation interface. The reduced entity count does not affect the validity of our comparative analysis, as both approaches face identical sparse observation challenges.

<sup>6</sup>Implementation must guarantee reliable data delivery and persistence—the question is not whether to provide these guarantees but how to implement them efficiently. Options range from consensus protocols and CRDTs.

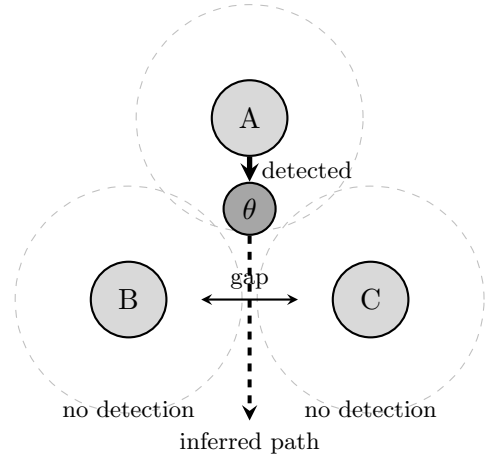


Figure 3: With  $\epsilon$ -nodes deployed at 1km resolution and 200 m detection radius, significant blind spots exist between coverage areas. The GNN must leverage the absence of detections at sensors B and C, combined with sensor A’s observation, to infer that entity  $\theta$  likely traversed the gap between the sensors’ coverage zones.

ing away the DOB layer’s specific reliability mechanisms.

We also require perfect positional knowledge for all nodes via GPS, as specified by setting the RPR positional uncertainty parameter  $\delta_{\text{pos}} = 0$ . While this requirement may be challenging for low-power devices, we postulate that it is feasible to achieve accurate positioning (small  $\delta_{\text{pos}}$ ) through a combination of synchronized clocks, triangulation, and limited GPS access at  $\sigma$ -nodes. However, such implementation considerations lie beyond the scope of this study.

These abstractions allow us to isolate the effect of model choice—GNN versus Kalman filter.

### 2.4 Graph Construction

Each node type— $\epsilon$  and  $\theta$ —is associated with a 4-dimensional feature vector representing position  $(x, y)$  and velocity  $(\Delta x, \Delta y)$ . These features are computed as averages over a context window - 60-ticks<sup>7</sup> in the case of the experiments we ran.

The edge structure includes: **Communication edges** (communicates:  $\epsilon \rightarrow \epsilon$ ) which

<sup>7</sup>each tick represents 10.7s of realtime

represent sensor connectivity. Sensors connect based on a Delaunay-Voronoi mesh topology (which we describe in subsection 2.6) forming the backbone of the network’s information flow. **Detection edges** (`detects`:  $\varepsilon \rightarrow \theta$ ) represent past observations, linking sensors to entities detected within the SCV configured sensing radius (set at 200 m in our experiments). **Prediction target edges** (`will_detect`:  $\varepsilon \rightarrow \theta$ ) encode future detections that the model is trained to predict—present in the ground truth but excluded from the input graph during training.

To capture temporal dynamics, we construct one graph per prediction window, generating targets at three distinct horizons: 30 ticks (short-term), 100 ticks (medium-term), and 150 ticks (long-term). This setup allows us to evaluate how model performance degrades with increasing prediction difficulty.

## 2.5 Motion Models

Marine entity movements in our simulation follow species-specific motion patterns designed to produce complex, deterministic trajectories governed by hidden rules. While not biologically realistic, these patterns ensure movements have underlying structure that models can potentially learn, rather than being purely random or following a known formula. This allows us to evaluate model performance across a range of different kinds of movement to reduce bias from overfitting to a single trajectory class when comparing models.

For **fish**, including European seabass (*Dicentrarchus labrax*) and Atlantic horse mackerel (*Trachurus trachurus*), we model movement as a combination of passive drift and active swimming:

$$\Delta \mathbf{x} = \mathbf{v}_{curr} + \boldsymbol{\epsilon} \quad (1)$$

where  $\mathbf{v}_{curr}$  represents the local ocean current velocity and  $\boldsymbol{\epsilon} \sim \mathcal{N}(0, \eta_{fish}^2 \mathbf{I})$  captures random swimming behavior, with  $\eta_{fish} = 0.05$  km. This formulation produces the characteristic random-walk patterns observed in schooling fish, with schools generally following current flows while exhibiting small-scale deviations driven by feeding or social behaviors.

**Cetaceans**, such as bottlenose dolphins (*Tursiops truncatus*), follow more structured

trajectories that reflect their higher cognitive abilities and purposeful movement patterns:

$$\mathbf{x}(t) = \mathbf{x}_0 + vt\hat{\mathbf{n}} + A \sin(\omega t)\hat{\mathbf{n}}_{\perp} \quad (2)$$

Here, dolphins maintain a consistent swimming speed  $v = 0.15$  km/tick along a primary direction  $\hat{\mathbf{n}}$ , while executing sinusoidal deviations with amplitude  $A = 0.5$  km perpendicular to their travel direction ( $\hat{\mathbf{n}}_{\perp}$ ).

**Ocean currents** are simulated using Perlin noise fields [18]. This approach creates spatially correlated flow patterns that evolve smoothly over time, mimicking the large-scale circulation patterns and smaller eddies found in real marine environments. All mobile nodes—both sensors and entities—experience these currents, leading to correlated drift patterns that challenge simplistic tracking assumptions.

## 2.6 Network Topology

The `communicates` ( $\varepsilon \rightarrow \varepsilon$ ) relationship is established with a Delaunay-Voronoi hybrid mesh [19]. We chose this design to maximize  $\varepsilon$ -node power efficiency.

At deployment, we initialize the network using **Delaunay triangulation** [20], as shown in Figure 4a. This construction connects sensors into triangles where no sensor lies within any triangle’s circumcircle, yielding maximally equiangular triangles that avoid long, thin connections—critical for minimizing transmission power requirements.

As sensors drift with ocean currents, we leverage **Voronoi diagrams** to efficiently update the network topology. Figure 4b illustrates how Voronoi cells partition the ocean surface into convex regions, each containing all points closest to a single sensor [21]. We exploit the duality between these structures: sensors are Voronoi neighbors if and only if they share a Delaunay edge. This duality enables localized topology updates every 2 hours—when a sensor detects drift beyond a threshold, it only needs to recalculate connections with its Voronoi neighbors rather than the entire network.

Edge formation follows three constraints:

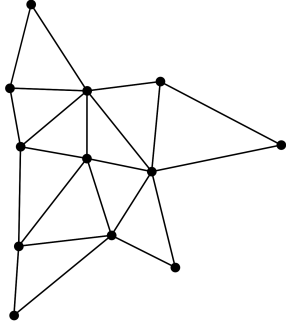
- **Energy:** At most 5 neighbors per  $\varepsilon$

- **Redundancy:** At least 3 neighbors per  $\varepsilon$
- **Range:** No edge longer than 10 km

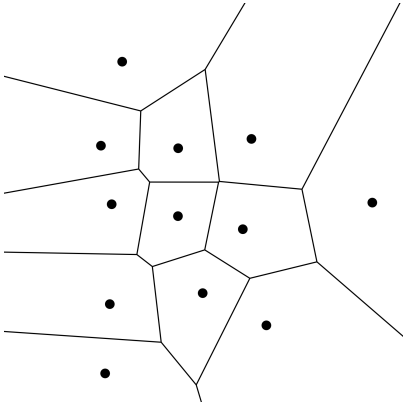
## 2.7 Technology Stack

The Aquascan framework is implemented in Python using **NumPy** for numerical computations and **Bokeh** for interactive visualization. Simulation data is stored in **HDF5** format with **OmegaConf** managing configuration parameters.

The GraphSAGE model is built with **PyTorch** (v2.0+) and **PyTorch Geometric**, featuring three convolution layers (64-dim hidden states, ReLU activation, batch normalization) operating on heterogeneous graphs with epsilon/theta nodes and communication/detection edges. Training uses binary cross-entropy loss with Adam optimization (lr=1e-3), while **scikit-learn** computes evaluation metrics.



(a) Delaunay triangulation at deployment



(b) Voronoi partitioning for dynamic updates

Figure 4: Network topology representations for the same set of 12  $\varepsilon$ -nodes. (a) Initial triangulation ensures no node lies within any triangle’s circumcircle. (b) Voronoi cells define spatial regions for neighbor discovery as nodes drift.

## 3 Methodology

### 3.1 Problem Formulation

To address our research question comparing GNNs and Kalman filters for marine trajectory prediction, we formulate the problem as a link prediction task on heterogeneous spatiotemporal graphs. Given a graph  $G_t = (V, E_t)$  at time  $t$  with node set  $V = V_\varepsilon \cup V_\theta$  representing sensors and entities respectively, and edge set  $E_t$  encoding current relationships, our objective is to predict future detection edges  $E_{t+\Delta t}$  for multiple prediction horizons  $\Delta t \in \{30, 100, 150\}$  ticks.

### 3.2 Heterogeneous GraphSAGE

We extend GraphSAGE to heterogeneous graphs with node types  $V = V_\varepsilon \cup V_\theta$  and edge types  $\mathcal{R} = \{\text{communicates}, \text{detects}, \text{rev\_detects}\}$ . Each node carries 4D features  $\mathbf{h}_v^{(0)} = [x, y, \Delta x, \Delta y]^T$  averaged over a 60-tick window.

The architecture employs type-specific input projections followed by three heterogeneous

convolution layers:

$$\mathbf{h}_v^{(l+1)} = \sigma \left( \mathbf{W}_{\text{self}}^{(l)} \mathbf{h}_v^{(l)} + \sum_{r \in \mathcal{R}} \sum_{u \in \mathcal{N}_r(v)} \mathbf{W}_r^{(l)} \cdot \text{MEAN}(\mathbf{h}_u^{(l)}) \right) \quad (3)$$

Each layer uses edge-type-specific SAGE-Conv operators (hidden dim=64) with ReLU activation and batch normalization. Link prediction employs dot-product decoding:

$$p_{ij} = \sigma(\mathbf{h}_i^{(3)} \odot \mathbf{h}_j^{(3)} \cdot \mathbf{1}) \quad (4)$$

We address detection sparsity through positive class weighting  $w_1 = |E^-|/|E^+|$  in the BCE loss. Implementation details and hyperparameters are provided in Appendix A and our repository<sup>8</sup>.

### 3.3 Kalman Filter Baseline

We implemented a classical tracking approach [22] using independent constant-velocity Kalman filters [23] for each marine entity as baseline. Each filter maintains a **4-dimensional state vector**  $\mathbf{x} = [x, y, v_x, v_y]^T$  encoding position and velocity, with dynamics governed by the standard linear motion model [24]. The **process noise covariance**  $\mathbf{Q}$  models random accelerations in the constant-velocity model. We systematically tuned the acceleration variance through grid search over  $q \in \{10^{-4}, 10^{-3}, 10^{-2}, 10^{-1}\}$  km<sup>2</sup>/tick<sup>2</sup>, selecting  $q = 10^{-2}$  based on validation set performance. The measurement noise variance was set to  $r = 0.01$  km<sup>2</sup> to reflect the localization uncertainty within the sensor’s detection radius<sup>9</sup>. Each Kalman filter operates independently, processing observations from its tracked entity without awareness of other entities or the sensor network topology. This independence—while computationally efficient—prevents the Kalman approach from leveraging the rich relational information.

<sup>8</sup><https://github.com/aquascan/aquascan-gnns>

<sup>9</sup>Since variance has squared units, position variance is expressed in km<sup>2</sup>. The value  $r = 0.01$  km<sup>2</sup> corresponds to a standard deviation  $\sigma = \sqrt{0.01} = 0.1$  km = 100 m, representing approximately half the 200 m detection radius—a reasonable localization uncertainty for entities detected within the sensor’s coverage area.

For prediction, the Kalman filters employ pure motion model extrapolation, propagating the state estimate forward using the constant velocity assumption.

### 3.4 Training & Evaluation

We trained the GNN using binary cross-entropy loss for the link prediction task, optimized with Adam at a learning rate of 0.001. Training ran in mini-batches of 32 graph snapshots, each representing a full heterogeneous graph for a given time window.

Early stopping with a patience of 10 epochs monitored validation loss. Training ran for up to 100 epochs, though convergence often occurred earlier. Data was split temporally: 70% for training, 15% for validation, and 15% for testing—each over contiguous intervals to preserve temporal structure.

The primary evaluation metric was AUC (Area Under the ROC Curve). We also reported precision and recall at selected thresholds to quantify false positives and misses.

As a sanity check, we visually inspected predicted trajectories to ensure both models produced physically plausible paths consistent with the underlying motion models (e.g., smooth continuous movement, reasonable velocities) rather than erratic or discontinuous predictions that would indicate implementation errors. To assess robustness across time horizons, we computed performance degradation as the relative AUC drop from short- to long-horizon predictions.

## 4 Experimental Setup

### 4.1 Simulation Environment

Our experiments used the Aquascan simulation framework to model a controlled marine sensing scenario over a **30 km × 16 km** oceanic region. We deployed **570  $\epsilon$ -nodes** in a hexagonal grid with approximately 1 km resolution.

To evaluate spatial resolution trade-offs, we tested alternative configurations. The hexagonal layout gives each node six neighbors and computes vertical spacing as:

$$\text{vertical spacing} = \frac{\sqrt{3}}{2} \times \text{horizontal spacing}$$

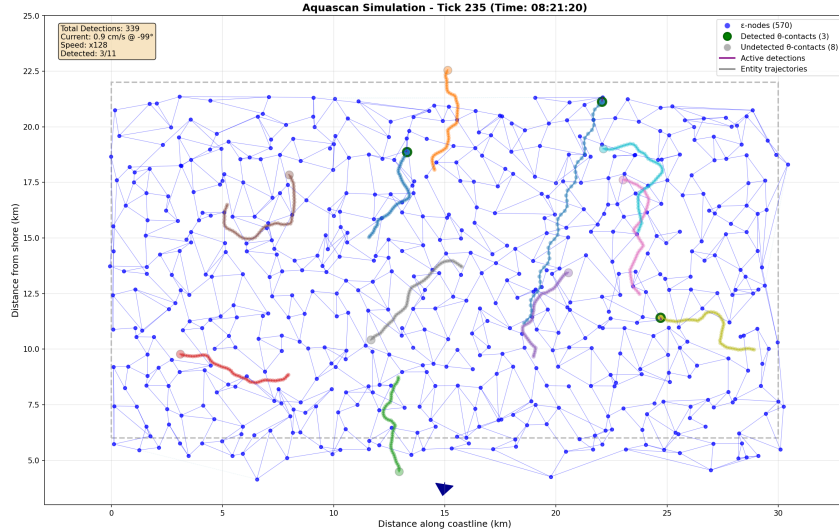


Figure 5: Representation of  $\theta$ -node movement within the Aquascan simulation framework.

Table 1: Dataset statistics across prediction horizons. Shorter horizons yield more training samples due to sliding window constraints.

Horizon	30-tick (5.3 min)	100-tick (17.8 min)	150-tick (26.7 min)
Total graphs	14,700	7,700	2,700
Training set	10,290	5,390	1,889
Validation set	2,205	1,155	405
Test set	2,205	1,155	406
Total predictions	13.8M	7.2M	2.5M
Dataset size	5.1 GB	2.7 GB	0.96 GB

Table 2: Detection grid resolution and  $\varepsilon$ -node count across grid granularities.

Grid Resolution	Horizontal Spacing	Vertical Spacing	Total Sensors
5 km	5.0 km	4.33 km	24
1 km	1.0 km	0.87 km	570
0.5 km	0.5 km	0.43 km	2,220
0.1 km	0.1 km	0.09 km	55,500

The initial hexagonal layout improves coverage efficiency, requiring 13.4% fewer nodes than a rectangular grid.

Then, the marine ecosystem is populated with **15-20  $\theta$ -nodes** representing different biological entities. Each simulation spans **24-hour periods** executed at **128x speed**, compressing a full diurnal cycle into manageable computational timeframes while capturing tidal variations and other time-dependent behaviors. Each time unit (each tick) represents 10.7 seconds of real-time, providing sufficient

temporal resolution to capture rapid maneuvers when  $\theta$ -nodes are in detection range.

Figure 5 illustrates a snapshot of the interactive simulation (Bokeh implementation in the repository), emphasising the  $\theta$ -node trajectories and the dynamic, rearranged mesh of  $\varepsilon$ -nodes, now departed from its original hexagonal layout.

## 4.2 Experimental Parameters

Building on the system architecture described in Section 2, we instantiate specific parameters for our comparative evaluation. The simulation generates approximately **1.2 million detection events** over **1,000 hours** of marine operations, partitioned temporally into disjoint sets: 700h for training, 150h for validation, and 150h for testing.

Ocean currents in our simulation exhibit 6-hour tidal periodicity, matching semi-diurnal patterns common in coastal regions. Network

topology updates are evaluated  $T_{reconfig} = 2$  hours intervals, triggered by accumulated sensor drift exceeding positional thresholds.

For graph construction, we extract overlapping temporal windows from the continuous simulation:

$$G_i = \text{GraphExtract}(t_i, t_i + W_{context}) \quad (5)$$

where  $W_{context} = 60$  ticks defines the historical context, and windows begin at:

$$t_i = i \cdot s, \quad s = \begin{cases} 10 \text{ ticks} & \text{during training} \\ 30 \text{ ticks} & \text{during evaluation} \end{cases} \quad (6)$$

The multi-horizon evaluation defines prediction targets at  $\Delta t \in \{30, 100, 150\}$  ticks beyond each context window. Given our  $128\times$  simulation speed where each tick represents 10.7 seconds of real time, these horizons correspond to approximately 5, 17, and 25-minute forecasts. This design exposes how prediction methods degrade with temporal distance: short horizons primarily test motion model accuracy, while longer horizons demand reasoning about network-wide patterns—revealing fundamental differences between local (Kalman) and relational (GNN) approaches.

### 4.3 Dataset Construction and Scale

We generated **100 independent 24-hour simulations** with different random seeds. To handle the computational demands of processing millions of spatio-temporal interactions, we implemented a parallelized pipeline leveraging multi-core CPUs and GPU acceleration, requiring over **40 compute-hours** when accounting for all processes.

Our multi-horizon graph construction pipeline transformed this raw simulation data into three prediction datasets:

The decreasing sample counts reflect the temporal constraints of our sliding window approach—each graph requires 60 ticks of historical context plus the full prediction horizon of future data. To address the extreme class imbalance inherent in detection (positive events comprise only 0.065% of samples), we computed class weights dynamically, ranging from 1,534:1 for short horizons to 364:1 for long horizons.

Experiments utilized cloud infrastructure with an NVIDIA T4 GPU (16GB VRAM) and high-memory configuration (32GB system memory). This computational setup enabled efficient training of our GraphSAGE models, with convergence typically achieved within 4 hours per configuration. Inference latency remained below 50ms per prediction, comparing favorably to existing marine monitoring systems where "real-time" acoustic detection typically operates on timescales of seconds to hours [25]. This millisecond-scale latency demonstrates the feasibility of truly real-time deployment in marine monitoring applications.

## 5 Results

Our experiments reveal fundamental differences in how graph neural networks and traditional Kalman filters handle the challenges of sparse sensor coverage and heterogeneous marine environments. Across 100 independent simulations totaling over 25,000 spatio-temporal graphs, we evaluated both approaches on their ability to predict future detection events and maintain realistic trajectory patterns. The results demonstrate a clear performance hierarchy: while both methods achieve similar accuracy for short-term predictions where simple motion models suffice, their capabilities diverge dramatically as prediction horizons extend and the complexity of leveraging distributed sensor information becomes paramount.

### 5.1 GNNs Outperform Kalman Filters Across All Prediction Horizons

We evaluated prediction accuracy across 100 independent 24-hour simulations, processing over 25,000 spatio-temporal graphs.

As shown in Figure 6, **both methods achieve comparable short-term prediction accuracy** (0.968 vs 0.970 AUC at 30 ticks,  $p = 0.23$ ), however, their performance diverges significantly at longer horizons. **The GNN maintains 0.952 AUC at 150-tick forecasts, while Kalman filter performance degrades to 0.694.**

Table 3: AUC comparison between Kalman and GNN models across prediction horizons

Horizon	Kalman	GNN	p-value
30t	0.968	0.970	0.23
100t	0.775	0.963	<0.001
150t	0.694	0.952	<0.001

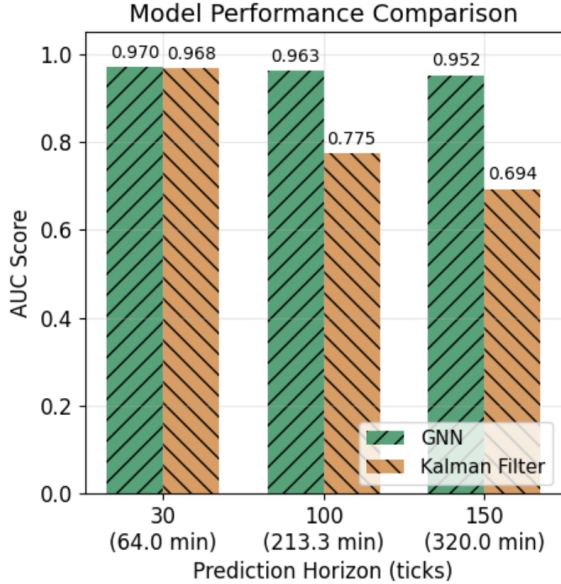


Figure 6: Side-by-side comparison of Area Under the ROC Curve (AUC) performance between Graph Neural Networks and Kalman Filter across three prediction horizons (30, 100, 150 ticks). GNN maintains 95-97% AUC across all horizons while Kalman performance degrades sharply from 97% to 69% as horizon increases.

The performance degradation analysis (Figure 7) reveals fundamentally different scaling behaviors. The Kalman filter exhibits linear performance decay (28% drop from 30 to 150 ticks), while the GNN maintains near-constant performance (2% degradation). This translates to an average improvement of 21% over the Kalman baseline across all horizons.

## 5.2 GNNs Maintain Trajectory Coherence in Complex Motion Patterns

The GNN maintained realistic trajectories for all entity types, preserving characteristic sinusoidal patterns for dolphins and random-walk current-influenced behaviors for fish schools.

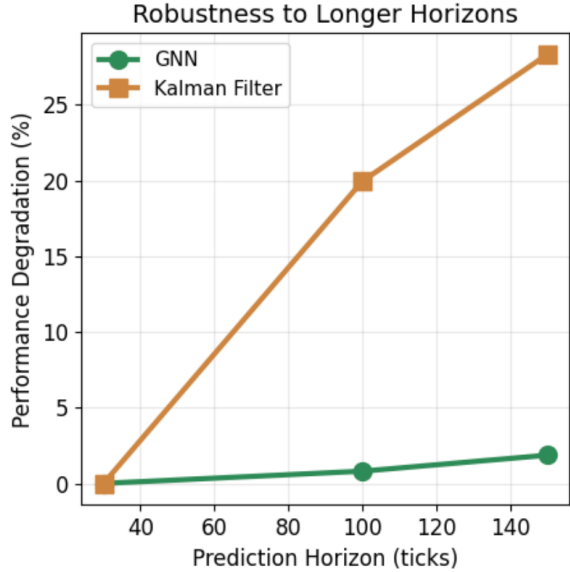


Figure 7: Relative performance degradation from baseline (30-tick) performance as prediction horizon increases. GNN shows minimal degradation (2% drop) while Kalman filter exhibits severe degradation (28% drop).

In contrast, Kalman filters often linearized into unrealistic straight-line extrapolations after losing sensor contact.

The remarkable difference in prediction accuracy between methods—with GNN maintaining 95.2% AUC versus Kalman’s 69.4% at 150-tick horizons—strongly suggests that the GNN successfully learns and exploits these species-specific motion patterns. The GNN’s ability to leverage multi-hop information propagation through the sensor network enables accurate predictions even during extended observation gaps, effectively learning the underlying movement dynamics from the collective observations across the entire network.

**To what extent do GNNs maintain trajectory coherence?** While our results demonstrate clear superiority in prediction accuracy, precisely quantifying the degree to which GNNs capture specific motion characteristics remains an open question. Future work should systematically compare detection performance across varying levels of movement complexity—from purely random walks to deterministic trajectories—to establish a more nuanced understanding of how network topology and motion patterns interact to enable accurate long-term predictions. What is clear

from our experiments is that the GNN’s relational reasoning provides a fundamental advantage over traditional independent tracking approaches, particularly as prediction horizons extend beyond immediate sensor coverage.

These findings conclusively demonstrate the superiority of graph neural networks for marine tracking in sparse sensor networks. The GNN’s consistent 95%+ AUC performance across all time horizons, combined with its ability to maintain realistic trajectory patterns, establishes it as a transformative approach for next-generation marine monitoring systems. Where traditional Kalman filters fail due to their inability to leverage network-wide information, GNNs excel by treating the tracking problem as it truly is: a collective sensing challenge best solved through relational reasoning across the entire sensor network.

## 6 Related Work

### 6.1 Traditional Marine Trajectory Prediction

Maritime trajectory prediction has a rich history rooted in statistical signal processing. The field’s foundation was established by Kalman’s seminal 1960 filter paper [23], which provided the fundamental algorithm for state estimation in noisy environments. This approach has been extensively adapted for maritime applications, particularly in vessel tracking where it processes noisy sensor data to maintain coherent trajectory estimates [12, 26]. Modern implementations demonstrate the maturity of these classical methods. Extended and Unscented Kalman Filter variants successfully track vessels using Automatic Identification System (AIS) data, interpolating missing positions and providing reliable short-term predictions [13, 14]. The integration of multiple sensor modalities—radar, sonar, and AIS—through sensor fusion architectures has further enhanced tracking accuracy [27]. Particularly noteworthy is Fossen’s comprehensive framework for marine vehicle guidance and control [28], which established mathematical models for vessel dynamics that remain widely used. These statistical approaches excel in scenarios with cooperative targets broadcasting

regular position updates. Recent dual Kalman configurations have pushed the boundaries of prediction horizons [15], though challenges remain when modeling complex biological motion patterns or extended forecast windows.

### 6.2 Graph Neural Networks for Maritime Applications

The application of Graph Neural Networks to maritime domains represents a paradigm shift in how we model vessel interactions and movement patterns. Building on the theoretical foundations established by Battaglia et al. [29], maritime researchers have recognized that vessel movements are inherently relational—ships influence each other’s trajectories through collision avoidance, convoy formations, and port traffic patterns. This insight has led to impressive advances in vessel trajectory prediction. GNNs naturally capture the spatiotemporal dependencies between vessels by representing them as nodes in a dynamic graph, with edges encoding various relationships such as proximity, similar routes, or shared destinations [30, 31]. Recent architectures have demonstrated particular success in congested waterways, where vessel-to-vessel interactions strongly influence movement decisions [32, 33]. The graph-based approach has proven especially valuable for port traffic prediction, where the structured nature of shipping lanes and berth assignments creates natural graph topologies. These models learn complex patterns from the sensor network topology itself, achieving significant improvements over traditional independent tracking methods [34]. The success of these approaches in cooperative vessel tracking suggests promising potential for other maritime monitoring applications.

### 6.3 Marine Sensing Systems and Challenges

Marine sensing has evolved dramatically from its military origins in systems like SOSUS [35] to today’s diverse ecosystem of monitoring technologies. The theoretical foundations for underwater acoustic sensing were established by Wenz’s characterization of ocean ambient noise [36] and Urick’s comprehensive treatment of underwater sound princi-

ples [37], which remain standard references for system design. Modern marine life monitoring builds on Richardson et al.’s foundational work on marine mammals and noise [38], which established frameworks for passive acoustic monitoring still used today. Contemporary systems employ distributed networks of low-cost sensors utilizing various detection modalities—acoustic, optical, and electromagnetic—to monitor marine ecosystems [39–41]. Projects like INSTINCT have successfully detected and classified millions of marine mammal calls, demonstrating the maturity of passive acoustic monitoring [42]. The evolution toward distributed sensor networks was anticipated by Akyildiz et al.’s comprehensive survey of underwater sensor networks [43], which identified key challenges including limited bandwidth, propagation delays, and sensor mobility. Modern implementations address these challenges through innovative approaches to power management, communication protocols, and data processing [44–46]. While significant progress has been made, operational deployments still contend with sensor drift, intermittent connectivity, and energy constraints—factors that influence system design and data quality [47].

## 6.4 Deep Learning Advances in Maritime Prediction

Recent comprehensive reviews document how data-driven approaches now routinely outperform classical methods for vessel trajectory prediction [48]. This transformation reflects the field’s recognition that maritime movement patterns often exhibit complex, non-linear dynamics best captured through learning-based approaches. Innovative architectures tailored to maritime challenges have emerged across multiple fronts. Hybrid deep learning models combine the strengths of different neural network types to handle the unique characteristics of maritime data [49]. Spatiotemporal GNNs designed specifically for coastal environments account for geographic constraints and tidal influences [50, 51]. Specialized trajectory prediction networks incorporate domain knowledge about vessel behavior and maritime regulations [52, 53]. These advances are particularly relevant for challenging environments. The con-

sistent superiority of learning-based methods over traditional approaches, especially in scenarios with rich relational structure, validates the ongoing shift toward AI-driven maritime monitoring [54].

## 7 Discussion

The multi-hop message passing architecture of GNNs provides an important advantage: distributed sensor networks can aggregate information across multiple nodes to improve predictions. When direct observations are unavailable, our GNN can leverage indirect information—if sensor A detected northeastern movement and sensors B and C show no detections, the model learns to infer likely paths between coverage areas. This ability to utilize negative information (non-detections) distinguishes the graph-based approach from traditional filtering methods<sup>10</sup>.

Our results demonstrate that GNNs consistently outperform Kalman filters across all prediction horizons, maintaining 0.952 AUC at 150-tick forecasts while Kalman performance degrades to 0.694. This performance difference stems from GNNs’ ability to model both spatial relationships and temporal dependencies simultaneously, preserving non-linear trajectory characteristics. Where Kalman filters produce linear extrapolations under extended prediction horizons<sup>11</sup> [12, 47], GNNs maintain

<sup>10</sup>While our 2D surface tracking model abstracts depth considerations through the 200m detection radius (suitable for nearshore fishing areas), deep-diving species present additional challenges. The same topological principles could extend to 3D tracking networks, particularly for fixed structures like offshore platforms, where GNNs would learn vertical movement patterns. This introduces complexities in sensor placement, detection range modeling, and computational requirements that warrant dedicated investigation.

<sup>11</sup>While deploying more densely-spaced sensors could theoretically improve Kalman filter performance by reducing observation gaps, this approach faces practical limitations: deployment costs scale linearly with sensor count, environmental impact increases with physical infrastructure, and maintenance becomes prohibitively expensive for large-scale networks. In contrast, computational costs for GNNs are negligible by comparison and scale efficiently—our experiments processed 570 sensors on commodity datacenter hardware. The choice between dense sensor networks with simple algorithms versus sparse networks with intelligent processing reflects broader economic trends favoring computa-

trajectory coherence by encoding spatial context through their message-passing mechanism [29, 34].

**Data Acquisition and Learning Potential.** The network’s ability to learn from collective observations could enable detection of previously unidentified patterns in marine traffic or animal migration. With sufficient training data<sup>12</sup>, such systems might identify frequently used corridors or convergence zones. The Aquascan framework’s modular architecture supports investigation of how sensor density, network topology, and environmental noise affect tracking performance, following co-simulation best practices for complex system modeling [44–46]. Importantly, Aquascan need not remain purely synthetic—future versions could integrate real-world data streams, creating a digital twin ocean with a bidirectional relationship: the simulation improves the predictive model while real data helps refine the simulation. This approach aligns with broader trends in applying AI to marine environment prediction [54], where the ability to detect anomalies through learned patterns supports various monitoring applications.

The heterogeneous graph structure also opens opportunities for incorporating additional domain-specific relationships: environmental edges could capture how ocean currents or temperature gradients influence entity movements, while vessel interaction edges might model how shipping traffic affects marine life dispersal patterns. Such extensions would enable the system to learn complex cause-effect relationships—for instance, how commercial shipping lanes create barriers that

---

tional investment over physical infrastructure.

<sup>12</sup>Initial training data would be generated through controlled deployments in bounded environments—river systems for environmental impact assessments provide an ideal starting point with known entity populations and constrained geography. These deployments would combine temporary tagging campaigns with fixed sensor networks to establish ground truth, progressively scaling to coastal areas as the system learns characteristic movement patterns. Unlike traditional approaches requiring extensive tagging programs, the GNN approach needs only enough labeled data to bootstrap learning; thereafter, the network can leverage the collective patterns from millions of unlabeled detections to refine its predictions.

fragment whale pods or how fish schools redistribute in response to vessel noise.

### Computational Requirements at Scale.

While our experiments successfully demonstrated GNN performance with 570 sensors—a realistic scale for coastal monitoring deployments—we acknowledge that computational requirements differ fundamentally from traditional approaches like Kalman filters. Our hierarchical architecture addresses these requirements through appropriate task distribution:  $\varepsilon$ -nodes function purely as data relays, performing only basic sensing and short-range communication with no ML inference at the edge. The  $\sigma$ -nodes aggregate sensor data and perform initial preprocessing, while  $\Omega$ -nodes (datacenters) handle the computationally intensive GNN inference. Unlike Kalman filters that can run locally on each sensor, GNNs require datacenter-grade computational resources. However, our experiments demonstrate that standard datacenter infrastructure is sufficient—we successfully processed 24-hour simulations with 570 sensors using modest computational budgets. The trade-off between local simplicity (Kalman filters) and centralized intelligence (GNNs) reflects the broader shift towards a data-driven economy where increased computational investment yields superior insights. This parallels trends across industries where organizations invest orders of magnitude more compute than a decade ago to extract value from distributed sensor networks. Moreover, the advent of offshore data processing capabilities, including underwater datacenters [16], could enable low-latency marine analytics directly at sea, opening new possibilities for real-time ecosystem monitoring and adaptive sampling strategies.

Our study has several limitations. We used synthetic data with simplified motion models rather than complex hydrodynamic simulations. While recent studies have quantified real trajectory patterns of aquatic species using various tracking technologies [55–58], we prioritized computational efficiency and controlled experimental conditions. Future work could leverage these empirical datasets for cross-validation or incorporate biologically-informed motion parameters to bridge the gap

between synthetic and real-world trajectories. The comparison focused on standard Kalman filters; more sophisticated tracking methods such as particle filters, Interacting Multiple Model (IMM) filters, or extended/unscented Kalman filter variants might show improved performance over the basic implementation tested. The link prediction formulation, while effective, doesn't fully capture continuous-time dynamics. While not a limitation of our simulation study, we acknowledge that real-world deployments would face additional challenges like biofouling, power constraints, and maintenance logistics that merit consideration for practical implementation. These findings nonetheless indicate that learning-based methodologies merit consideration for marine monitoring systems [59, 60] that routinely encounter measurement errors and noisy signals.

Future work should address several directions. Most critically, integration with real-world marine tracking datasets is essential to enrich the simulation framework beyond simple validation. While synthetic data enabled controlled comparison, incorporating actual sensor data and observed marine behaviors would provide the empirical grounding necessary to improve model fidelity and practical applicability. Additionally, comprehensive ablation studies should investigate which GNN components contribute most to performance improvements—examining the impact of network topology choices, message-passing depth, node feature selection, and edge type importance would inform more efficient architectures. Incorporating realistic biological behaviors through agent-based models and ocean dynamics from computational fluid dynamics would enhance simulation fidelity. Deploying prototype networks in controlled marine environments would validate our findings and identify implementation challenges. Advanced architectures incorporating temporal attention mechanisms and continuous-time modeling could improve long-horizon predictions. While we demonstrated strong performance with GraphSAGE, systematic evaluation of other GNN architectures—including Graph Attention Networks (GAT), Graph Convolutional Networks (GCN), Graph Isomorphism Networks (GIN), and Gated Graph Neural Net-

works (GGNN)—could identify architecture-specific advantages for marine trajectory prediction. Comparison with more sophisticated tracking baselines, including particle filters and IMM approaches, would provide a more comprehensive performance assessment. This performance advantage has been observed across various GNN architectures applied to spatiotemporal prediction tasks [30, 32, 51, 52].

This research demonstrates that graph neural networks can effectively leverage sparse, distributed marine observations to maintain tracking performance where traditional methods degrade, warranting further investigation of these methods in real-world marine monitoring deployments.

## 7.1 Robustness to Real-World Uncertainties

We acknowledge that our simplifying assumptions—particularly perfect positional knowledge ( $\delta_{\text{pos}} = 0$ ) and abstraction of communication failures—limit direct generalization to real-world deployments where uncertainty is intrinsic. In practice, positional errors would manifest as noisy node features, incorrect edge formation in the Delaunay-Voronoi topology, and misaligned detection events. Communication failures would result in missing edges and incomplete observation sequences. Similarly, our abstraction of data persistence layers ignores real-world challenges such as buffer overflows during network partitions and data corruption from harsh marine conditions.

Importantly, these simplifications apply equally to both the GNN and Kalman filter approaches, preserving the validity of our comparative analysis. The abstractions of reliable communication and perfect data persistence are orthogonal to the choice of tracking algorithm—both approaches would need to handle packet loss, routing delays, and storage constraints in a real deployment. However, we hypothesize that GNNs may demonstrate greater robustness to uncertainties in the sensing and detection aspects for three reasons: (i) their learned representations can implicitly compensate for systematic errors without requiring explicit noise models, (ii) they naturally handle varying graph structures arising from communication failures through their message-passing

architecture, and (iii) as demonstrated in Figure 3, they can reason about non-detections to infer entity presence despite coverage gaps.

While empirical validation awaits deployment of real distributed marine sensor networks, future work could investigate these effects through controlled experiments: introducing Gaussian positional noise ( $\delta_{\text{pos}} \sim \mathcal{N}(0, \sigma_{\text{pos}}^2)$ ), randomly dropping edges to simulate communication failures with probability  $p_{\text{fail}}$ , and adding temporal misalignment to model clock drift. Crucially, traditional tracking approaches such as Kalman filters, particle filters, and multiple hypothesis tracking would require explicit modeling of each uncertainty source—tuning process noise covariance matrices, defining detection likelihood functions for varying environmental conditions, and hand-crafting state transition models for different visibility or current conditions. In contrast, GNNs can learn these complex relationships directly from data: for instance, they might implicitly learn that detection probability decreases during high turbidity events or that strong currents increase positional uncertainty, without requiring domain experts to explicitly formulate these relationships mathematically. This data-driven approach is particularly valuable in marine environments where the interactions between environmental factors and sensor performance are complex and poorly understood.

Beyond positional and communication uncertainties, measurement errors and noisy signals are endemic to marine sensing due to multipath propagation, temperature-induced sound speed variations, and biological noise sources. While our simulation assumed perfect detection within the 200m radius, real acoustic sensors experience degraded performance from environmental factors: shipping noise can mask detection signals, thermoclines refract acoustic paths, and marine growth attenuates signal strength. We hypothesize that GNNs would demonstrate superior performance in these noisy conditions because they can learn to weight information from multiple sensors based on reliability patterns observed during training. For example, a GNN might learn to discount detections from sensors near shipping lanes during high-traffic periods or to rely more

heavily on sensors positioned away from known noise sources. This adaptive weighting emerges naturally from the attention mechanisms in graph neural networks, whereas traditional filters would require manual tuning of measurement noise covariance matrices for each sensor under varying conditions—an impractical task for large-scale deployments.

### Sensor Drift and Irregular Placement.

A fundamental advantage of GNNs over traditional tracking methods lies in their ability to handle irregular and dynamic sensor configurations. Traditional Kalman filters assume either fixed sensor positions or perfectly known sensor trajectories [61], requiring explicit coordinate transformations when sensors move [62]. In contrast, GNNs naturally adapt to changing graph topologies through their message-passing architecture [63, 64]. This distinction becomes critical in marine environments where sensors drift with ocean currents, creating constantly evolving network geometries.

Recent advances in graph neural networks demonstrate their superiority in handling dynamic topologies and missing sensors. GraphSAGE, the architecture we employ, uses inductive learning to generate embeddings for previously unseen node configurations without retraining [65]. Studies on sensor networks have shown that GNNs can maintain performance despite topology changes, sensor failures, and irregular placements [66, 67]. The Adaptive Feature and Topology Graph Convolutional Network (AAGCN) explicitly learns optimal graph structures from data, outperforming methods that rely on predefined topologies [68]. For marine tracking, this means GNNs can learn spatial relationships from the data itself rather than requiring precise sensor position knowledge—they discover which sensors provide reliable information under different environmental conditions and adaptively weight their contributions.

**Dynamic Topology Management.** While the GNN handles prediction despite sensor drift, our Voronoi-based topology management (Section 2.3) addresses practical network maintenance. As sensors drift with currents, some may converge due to similar flow patterns.

When sensors come within close proximity, the system has two options: (1) leverage redundant detections for validation, potentially improving detection confidence through corroboration, or (2) place redundant sensors in sleep mode to conserve battery. The dynamic Voronoi tessellation automatically identifies such proximity events every 2 hours, enabling adaptive resource management. This differs from traditional fixed-topology networks that cannot exploit or mitigate sensor convergence. During storm events or strong currents that compress sensor spacing, the network can dynamically adjust detection thresholds or duty cycles based on local sensor density, maintaining coverage while optimizing energy consumption.

## 8 Conclusion

Our work extends established maritime monitoring research into the challenging domain of non-cooperative biological entity tracking using distributed passive sensors. We differ from prior research in three fundamental ways: (i) we track biological entities with complex, non-linear motion patterns lacking explicit navigational intent, rather than vessels with transponders and predictable destinations; (ii) we employ distributed networks of small passive sensors instead of traditional centralized tracking stations; and (iii) we demonstrate how GNNs naturally handle irregular and dynamic sensor topologies—a critical capability when sensors drift with ocean currents, unlike traditional methods that assume fixed or perfectly known sensor positions.

This study benchmarked heterogeneous Graph Neural Networks (GNNs) against Kalman filters for predicting marine entity trajectories under these challenging conditions. GNNs demonstrated statistically significant performance improvements, maintaining 0.952 AUC at 150-tick prediction horizons compared to 0.694 for Kalman filters. This improved performance stems from GNNs’ ability to leverage network topology and aggregate information across multiple sensors, crucially adapting to irregular sensor placements and dynamic topologies without requiring explicit position knowledge or coordinate transformations—capabilities that become essential

as sensors drift with ocean currents throughout deployment.

The Aquascan simulation environment enabled controlled evaluation through standardized Spatiotemporal Contact Volume analyses, demonstrating that GNN performance remains stable even with sparse observations. These results indicate that heterogeneous GNNs provide an effective approach for trajectory prediction in distributed marine monitoring systems with intermittent connectivity and limited observations.

By providing an open-source benchmarking framework and quantitative performance comparisons, this work contributes to the application of graph-based learning methods in maritime contexts. The Aquascan simulation framework readily supports sensitivity analyses across different sensor densities, intermittent observation rates, and additional marine movement patterns—investigations we defer to future work. Our immediate priorities focus on: (i) evaluating alternative GNN architectures and emerging graph-based methods to push performance boundaries, and (ii) deploying real-world prototypes to validate our findings under uncontrolled marine conditions with natural noise sources and environmental variability. Such field deployments will ultimately demonstrate whether the promising simulation results translate to practical advantages in operational marine monitoring systems.

## Data and Code Availability

The Aquascan simulation framework and all code for reproducing the experiments in this paper are publicly available at: <https://github.com/ctvc-pt/aquascan-gnns>. The repository includes the complete simulation environment, model implementations, and notebooks for analysis. A snapshot of the version used in this paper has been archived at Zenodo with DOI: 10.5281/zenodo.15691882 for long-term preservation and citation.

## Acknowledgements

We thank the PRODEI Doctoral Program at the Faculty of Engineering, University of

Porto, and CTVC (a tech cooperative in northern Portugal) for their support and collaboration. We also thank José Costa Pereira, Leonardo Silva, and Leonel Nunes for their valuable insights.

## References

- [1] Arthur G. Cosby, Venustiano Lebakula, Christine N. Smith, Hasanat Alamgir, G. T. Bufkin, J. Fedá, Arsham Alamian, Mohammad Heidari, and Marinelle Payton. Accelerating growth of human coastal populations at the global and continent levels: 2000–2018. *Scientific Reports*, 14:22489, 2024.
- [2] OECD. *The Ocean Economy in 2030*. OECD Publishing, Paris, 2016.
- [3] IEA. Offshore wind outlook 2019, 2019.
- [4] European Commission. Communication from the commission to the european parliament, the council, the european economic and social committee and the committee of the regions - delivering on the eu offshore renewable energy ambitions. Technical Report COM(2023) 668 final, European Commission, Brussels, 2023.
- [5] Maximilian Felix Schupp, Martina Bocci, Daniel Depellegrin, Andronikos Kafas, Zacharoula Kyriazi, Ivana Lukic, Angela Schultz-Zehden, Gesche Krause, Vincent Onyango, and Bela Hieronymus Buck. Toward a common understanding of ocean multi-use. *Frontiers in Marine Science*, 6:165, 2019.
- [6] Andrew B. Gill, Steven Degraer, Andrew Lipsky, Ninon Mavraki, Elizabeth Methratta, and Robin Brabant. Setting the context for offshore wind development effects on fish and fisheries. *Oceanography*, 33(4):118–127, 2020.
- [7] S. Bharany, S. Sharma, N. Alsharabi, E. Tag Eldin, and N.A. Ghamry. Energy-efficient clustering protocol for underwater wireless sensor networks facing challenges of distributed sensing. *Frontiers in Marine Science*, 10, 2023.
- [8] I. Ullah, F. Ali, A. Sharafian, A. Ali, H.M.Y. Naeem, and X. Bai. Underwater internet of things: Connectivity optimization for distributed environmental monitoring. *Frontiers in Marine Science*, 11, 2024.
- [9] FAO. The state of world fisheries and aquaculture 2022. Technical report, Food and Agriculture Organization of the United Nations, Rome, 2022.
- [10] NOAA Fisheries. Understanding illegal, unreported, and unregulated fishing. National Oceanic and Atmospheric Administration, 2023.
- [11] Daniel Pauly and Dirk Zeller. Catch reconstructions reveal that global marine fisheries catches are higher than reported and declining. *Nature Communications*, 7:10244, 2016.
- [12] Krzysztof Jaskólski. Automatic Identification System (AIS) dynamic data estimation based on discrete Kalman Filter (KF) algorithm. *Scientific Journal of Polish Naval Academy (Zeszyty Naukowe Akademii Marynarki Wojennej)*, 58(4(211)):71–87, 2017.
- [13] Sindre Fossen and Thor I. Fossen. Extended Kalman Filter design and motion prediction of ships using live Automatic Identification System (AIS) data. In *2nd European Conference on Electrical Engineering and Computer Science (EECS'18)*, Bern, Switzerland, 2018. IEEE.
- [14] Sindre Fossen and Thor I. Fossen. eXogenous Kalman Filter (XKF) for visualization and motion prediction of ships using live Automatic Identification System (AIS) data. *Modeling, Identification and Control*, 39(4):233–244, 2018.
- [15] T. Zhou, D. Jiang, Z. Lin, G. Han, X. Xu, and J. Qin. Hybrid dual Kalman filtering model for short-term traffic flow forecasting. *IET Intelligent Transport Systems*, 13(6):1023–1032, 2019.
- [16] Ben Cutler, Spencer Fowers, Jeffrey Kramer, and Eric Peterson. Want an

- energy-efficient data center? build it underwater. *IEEE Spectrum*, 54(3):46–52, March 2017.
- [17] Marc Shapiro, Nuno Preguiça, Carlos Baquero, and Marek Zawirski. Conflict-free replicated data types. In Xavier Défago, Franck Petit, and Vincent Villain, editors, *Stabilization, Safety, and Security of Distributed Systems (SSS)*, volume 6976 of *Lecture Notes in Computer Science*, pages 386–400. Springer Berlin Heidelberg, 2011.
- [18] Ken Perlin. An image synthesizer. *ACM SIGGRAPH Computer Graphics*, 19(3):287–296, 1985. Seminal paper introducing Perlin noise to computer graphics.
- [19] Barry Joe and Carl A. Wang. Duality of constrained Voronoi diagrams and Delaunay triangulations. *Algorithmica*, 9:142–155, 1993. Establishes the mathematical relationship between constrained Voronoi diagrams and Delaunay triangulations.
- [20] Boris Delaunay. Sur la sphere vide. *Bulletin de l’Académie des Sciences de l’URSS*, 6:793–800, 1934.
- [21] Georgy Voronoi. Nouvelles applications des paramètres continus à la théorie des formes quadratiques. *Journal für die reine und angewandte Mathematik*, 134:198–287, 1908.
- [22] Yaakov Bar-Shalom, X. Rong Li, and Thiagalingam Kirubarajan. *Estimation with Applications to Tracking and Navigation: Theory, Algorithms and Software*. John Wiley & Sons, New York, 2001. Comprehensive treatment of tracking algorithms including Kalman filters and motion models.
- [23] Rudolph Emil Kalman. A new approach to linear filtering and prediction problems. *Journal of Basic Engineering*, 82(1):35–45, 1960.
- [24] Yaakov Bar-Shalom and Xiao-Rong Li. *Estimation and Tracking: Principles, Techniques, and Software*. Artech House, Boston, 1993. Standard reference for constant velocity and other motion models in tracking.
- [25] Marion Poupard, Maxence Ferrari, Jana Schlüter, Ricard Marxer, Pascale Giraudet, Valentin Barchasz, Valentin Gies, Gianni Pavan, and Hervé Glotin. Real-time continuous acoustic monitoring of marine mammals in the mediterranean sea. *Journal of Marine Science and Engineering*, 9(12):1389, 2021. Reviews real-time and near real-time acoustic monitoring systems where detection typically operates on timescales of seconds to hours.
- [26] Lokukaluge Prasad Perera, Paulo Jorge Ramalho Oliveira, and Carlos Guedes Soares. Maritime traffic monitoring based on vessel detection, tracking, state estimation, and trajectory prediction. *IEEE Transactions on Intelligent Transportation Systems*, 13(3):1188–1200, 2012.
- [27] S.W. Martin, B. Matsuyama, T.A. Helble, C.R. Martin, E.E. Henderson, and G.C. Alongi. Automated real-time detection and localization of marine mammals at the pacific missile range facility. *Journal of the Acoustical Society of America*, 144(3):1711, 2018.
- [28] Thor I. Fossen. *Guidance and Control of Ocean Vehicles*. John Wiley & Sons, Chichester, UK, 1994.
- [29] Peter W. Battaglia, Jessica B. Hamrick, Victor Bapst, Alvaro Sanchez-Gonzalez, Vinicius Zambaldi, Mateusz Malinowski, Andrea Tacchetti, David Raposo, Adam Santoro, Ryan Faulkner, Caglar Gulcehre, Francis Song, Andrew Ballard, Justin Gilmer, George Dahl, Ashish Vaswani, Kelsey Allen, Charles Nash, Victoria Langston, Chris Dyer, Nicolas Heess, Daan Wierstra, Pushmeet Kohli, Matt Botvinick, Oriol Vinyals, Yujia Li, and Razvan Pascanu. Relational inductive biases, deep learning, and graph networks. *arXiv preprint arXiv:1806.01261*, 2018.
- [30] Bing Yu, Haoteng Yin, and Zhanxing Zhu. Spatio-temporal graph convolutional net-

- works: A deep learning framework for traffic forecasting. In *27th International Joint Conference on Artificial Intelligence (IJCAI)*, pages 3634–3640, 2018.
- [31] Abdullallah Mohamed, Kun Qian, Mohamed Elhoseiny, and Christian Claudel. Social-STGCNN: A social spatio-temporal graph convolutional neural network for human trajectory prediction. In *IEEE/CVF Conference on Computer Vision and Pattern Recognition (CVPR)*, pages 14424–14432, 2020.
- [32] Xiliang Zhang, Jin Liu, Peizhu Gong, Chengcheng Chen, Bing Han, and Zhong-dai Wu. Trajectory prediction of seagoing ships in dynamic traffic scenes via a gated spatio-temporal graph aggregation network. *Ocean Engineering*, 287:115886, 2023.
- [33] H. Feng, G. Cao, H. Xu, and S.S. Ge. IS-STGCNN: An improved social spatio-temporal graph convolutional neural network for ship trajectory prediction. *Ocean Engineering*, 266:112960, 2022.
- [34] Jie Zhou, Ganqu Cui, Shengding Hu, Zhengyan Zhang, Cheng Yang, Zhiyuan Liu, Lifeng Wang, Changcheng Li, and Maosong Sun. Graph neural networks: A review of methods and applications. *AI Open*, 1:57–81, 2021.
- [35] Edward C. Whitman. Sosus: The secret weapon of undersea surveillance. In *To Use the Sea: Readings in Seapower and Maritime Affairs*, pages 252–263. Naval Institute Press, Annapolis, MD, 2001.
- [36] Gordon M. Wenz. Acoustic ambient noise in the ocean: Spectra and sources. *The Journal of the Acoustical Society of America*, 34(12):1936–1956, 1962.
- [37] Robert J. Urick. *Principles of Underwater Sound*. McGraw-Hill, New York, 3rd edition, 1983.
- [38] W. John Richardson, Charles R. Greene Jr., Charles I. Malme, and Denis H. Thomson. *Marine Mammals and Noise*. Academic Press, San Diego, CA, 1995.
- [39] G. J. Lowes, J. Neasham, R. Burnett, B. Sherlock, and C. C. Tsimenidis. Passive acoustic detection of vessel activity by low-energy wireless sensors. *Journal of Marine Science and Engineering*, 10(2):248, 2022.
- [40] J. Crance, S. Grassia, and NOAA Team. INSTINCT: Infrastructure for noise and soundscape tolerant investigation using command line toolbox, 2024. Successfully detected and classified 18 million fin whale calls from 25+ mooring sites over 13 years.
- [41] C.C. Wall, M. McKenna, L.T. Hatch, S.M. Van Parijs, and others. Sound cooperative (soundcoop): Community-focused cyber-infrastructure for marine pam data processing, 2024. Processing petabytes of data from distributed sensors globally.
- [42] Jessica L. Crance, Catherine L. Grassia, and NOAA Team. Instinct: Infrastructure for noise and soundscape tolerant investigation using command line toolbox. In *Proceedings of the Ocean Sciences Meeting*. AGU/ASLO/TOS, 2024. Successfully detected and classified 18 million fin whale calls from 25+ mooring sites over 13 years.
- [43] Ian F. Akyildiz, Dario Pompili, and Tommaso Melodia. Underwater acoustic sensor networks: Research challenges. *Ad Hoc Networks*, 3(3):257–279, 2005.
- [44] Cláudio Gomes, Casper Thule, David Broman, Peter Gorm Larsen, and Hans Vangheluwe. Co-simulation: A survey. *ACM Computing Surveys (CSUR)*, 51(3):1–33, 2019.
- [45] Z. Liu, Y. Chu, G. Li, and H. Zhang. Co-simulation system using vico for marine operations: Fmi-based framework with ai integration. 13765:260–275, 2023.
- [46] DNV GL and Kongsberg Maritime and NTNU and SINTEF Ocean. Open simulation platform: An open-source industry standard for maritime equipment co-simulation, 2020. Joint industry initiative with 20+ partners.
- [47] X. Zhang, J. Liu, P. Gong, C. Chen, B. Han, and Z. Wu. G-STGAN: Gated

- spatio-temporal graph aggregation network for ship trajectory prediction. *Transportation Research Part E: Logistics and Transportation Review*, 175:103152, 2023.
- [48] M. Zhang, P. Kujala, M. Musharraf, J. Zhang, and S. Hirdaris. A machine learning method for the prediction of ship motion trajectories in real operational conditions. *Ocean Engineering*, 283:114905, 2023.
- [49] X. Li, Y. Zhang, W. Chen, and H. Wang. Hybrid deep computing model for marine sensor data: Smoothing techniques with deep belief echo state networks. *IEEE Journal of Oceanic Engineering*, 50(1), 2025.
- [50] J. Kim, S. Lee, H. Park, and K. Choi. ST-GNN for coastal sea surface temperature prediction: Multivariate multi-step ahead forecasting. *Ocean Modelling*, 185:102234, 2023.
- [51] H. Zhang, X. Wang, Y. Liu, and Z. Chen. STZINB-GNN: Spatial-temporal zero-inflated negative binomial graph neural network for sparse maritime traffic data. *IEEE Transactions on Intelligent Transportation Systems*, 2024. Introduces sparsity parameter  $\pi$  using Zero-Inflated Negative Binomial distribution.
- [52] Daniel Holmberg, Ermo Clementi, and Teemu Roos. Seacast: A hierarchical graph-based deep learning model for high-resolution regional ocean forecasting. *arXiv preprint arXiv:2410.11807*, 2024. NeurIPS 2024 Workshop on Tackling Climate Change with Machine Learning.
- [53] J. Wang, X. Li, Y. Zhang, and H. Chen. STDGNN: Spatiotemporal dynamic graph neural network for regional vessel flow prediction. *Ocean Engineering*, 259:111897, 2022.
- [54] Tao Song et al. Artificial intelligence approaches for marine environment prediction: A comprehensive review. *Frontiers in Earth Science*, 11, 2023.
- [55] Eneko Aspillaga, Kiran Safi, Bernat Hereu, and Frederic Bartumeus. Performance of a novel system for high-resolution tracking of marine fish societies. *Animal Biotelemetry*, 9(1):1–14, 2021.
- [56] Valentina Di Santo, Elsa Goerig, Dylan K Wainwright, Otar Akanyeti, James C Liao, Theodore Castro-Santos, and George V Lauder. Convergence of undulatory swimming kinematics across a diversity of fishes. *Proceedings of the National Academy of Sciences*, 118(49):e2113206118, 2021.
- [57] Mattia Gazzola, Wim M Van Rees, and Petros Koumoutsakos. Scaling the tail beat frequency and swimming speed in underwater undulatory swimming. *Nature Communications*, 14(1):5596, 2023.
- [58] Martin Føre, Velimir Azvolinsky Solbakken, Karen Dregni Arnholt, Nina Bloecher, and Øyvind Pedersen. New concept for measuring swimming speed of free-ranging fish using acoustic telemetry and Doppler analysis. *Biosystems Engineering*, 220:103–113, 2022.
- [59] Q. Zhang, J. Li, M. Chen, and H. Wang. Spatial-temporal self-calibration for underwater acoustic networks with beacon drift. *IEEE Journal of Oceanic Engineering*, 48(2):456–470, 2023.
- [60] L. Wang, X. Chen, Y. Zhang, and H. Li. Hierarchical transmission framework for energy-efficient underwater wireless sensor networks. *Sensors*, 23(12):5759, 2023.
- [61] Rudolph Emil Kalman. A new approach to linear filtering and prediction problems. *Journal of Basic Engineering*, 82(1):35–45, 1960.
- [62] Paul W Miller, Jay A Farrell, Yanjun Zhao, and Vladimir Djapic. Unscented Kalman filter for long-distance vessel tracking in geodetic coordinates. *Ocean Engineering*, 260:111959, 2022.
- [63] Stefan Bloemheugel, Jurgen van den Hoogen, and Martin Atzmüller. A computational framework for modeling com-

- plex sensor network data using graph signal processing and graph neural networks in structural health monitoring. *Applied Network Science*, 6(1):1–23, 2021.
- [64] Dongxia Li, Fengning Jiang, Minggao Chen, and Tao Qian. Dynamic spatio-temporal graph network with adaptive propagation mechanism for multivariate time series forecasting. *Expert Systems with Applications*, 214:119374, 2023.
- [65] Will Hamilton, Zhitao Ying, and Jure Leskovec. Inductive representation learning on large graphs. In *Advances in Neural Information Processing Systems*, pages 1024–1034, 2017.
- [66] Shengzhong Liu, Shuochao Yao, Yifei Huang, Dongxin Liu, Huajie Shao, Yiran Zhao, Jinyang Li, Tianshi Wang, Ruijie Wang, Chaoqi Yang, et al. Handling missing sensors in topology-aware IoT applications with gated graph neural network. *Proceedings of the ACM on Interactive, Mobile, Wearable and Ubiquitous Technologies*, 4(3):1–31, 2020.
- [67] Jian Zhang, Shanghang Zhang, Guanhang Wu, José MF Moura, and Soumya Kar. Topology adaptive graph convolutional networks. *arXiv preprint arXiv:1710.10370*, 2021.
- [68] Yunfei Liu, Li Chen, Chuan He, Yong Peng, and Qing Ming. AAGCN: a graph convolutional neural network with adaptive feature and topology learning. *Scientific Reports*, 14(1):1–15, 2024.

## A Implementation Details

Table 4 summarizes the HeteroGraphSAGE architecture specifications. The model is implemented in PyTorch Geometric v2.0+ using the HeteroConv wrapper for handling multiple edge types. Node features are computed as rolling averages over 60-tick windows to capture local motion dynamics while filtering high-frequency noise.

Table 4: HeteroGraphSAGE architecture specifications

Component	Specification
Node types	$\varepsilon$ (sensors), $\theta$ (entities)
Edge types	communicates ( $\varepsilon \rightarrow \varepsilon$ ) detects ( $\varepsilon \rightarrow \theta$ ) rev_detects ( $\theta \rightarrow \varepsilon$ )
Input dimension	4 (position + velocity)
Hidden dimension	64
Convolution layers	3
Aggregation	Mean pooling
Activation	ReLU + BatchNorm
Decoder	Element-wise dot product
Loss	BCE with positive weighting
Optimizer	Adam (lr= $10^{-3}$ )
Batch size	32 graphs
Early stopping	Patience=10 epochs

The heterogeneous design allows relation-specific message passing: `communicates` edges propagate sensor network state, `detects` edges carry observation information, while `rev_detects` enables backpropagation of entity state to nearby sensors. Training graphs are constructed with all historical edges present but future `will_detect` edges excluded, preventing information leakage.

## B Simulation Snapshots

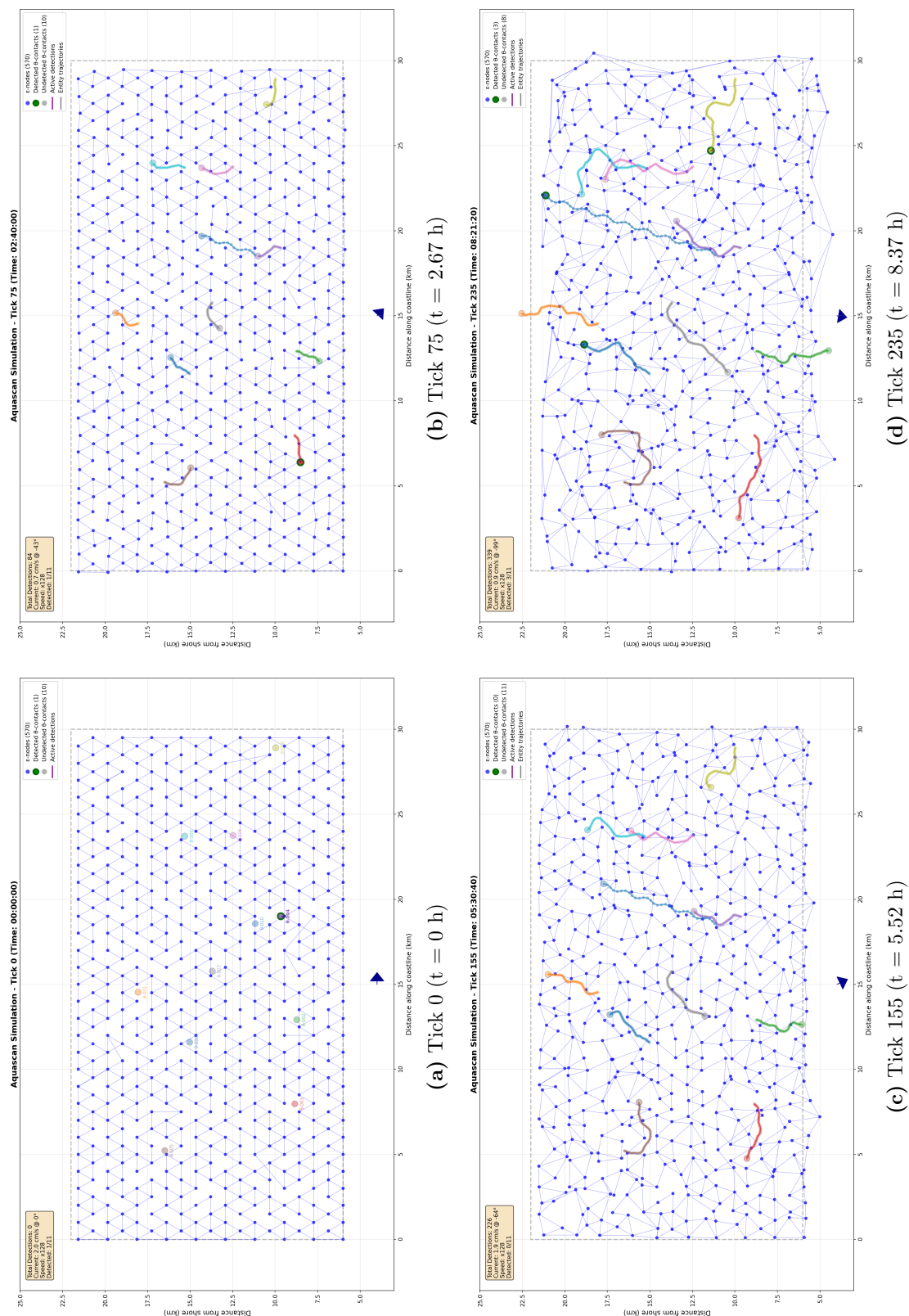


Figure 8: Temporal evolution of the Aquascan simulation over 8 hours.